CORE
Metadata, citation and similar papers at core.ac.uk
Provided by Repository of Faculty of Science, University of Zagreb

PHYSICAL REVIEW C **87**, 054606 (2013)

Quasielastic backscattering and barrier distributions for the ^{6,7}Li + ^{64}Zn systems

M. Zadro,[1,*] P. Figuera,[2] A. Di Pietro,[2] M. Fisichella,[2] M. Lattuada,[2,3] T. Lönnroth,[4] M. Milin,[5] V. Ostashko,[6] M. G. Pellegriti,[2,3] V. Scuderi,[2,3] D. Stanko,[5] E. Strano,[2,3] and D. Torresi[2,3]

[1]*Ruđer Bošković Institute, Bijenička cesta 54, HR-10000 Zagreb, Croatia*
[2]*INFN, Laboratori Nazionali del Sud, via S. Sofia 62, I-95123 Catania, Italy*
[3]*Dipartimento di Fisica e Astronomia, via S. Sofia 64, I-95123 Catania, Italy*
[4]*Physics, Department of Natural Sciences, Åbo Akademi, FI-20500 Åbo, Finland*
[5]*Faculty of Science of University of Zagreb, Bijenička cesta 32, HR-10000 Zagreb, Croatia*
[6]*Institute for Nuclear Research, Prospekt Nauki 47, UA-03680 Kiev, Ukraine*

(Received 5 April 2013; published 10 May 2013)

Excitation functions of quasielastic scattering at backward angles were measured for the weakly bound ^{6}Li and ^{7}Li projectiles on a ^{64}Zn target at energies around the Coulomb barrier. The corresponding barrier distributions were derived from the experimental cross sections. The experimental data were analyzed within the coupled-channel model using a double-folding potential as the bare potential. Inelastic excitations of the target, the ^{7}Li first-excited state, and ^{6,7}Li resonant state(s), corresponding to sequential breakup, were included in the calculations. The comparison between the data and coupled-channel predictions shows that the effects of channels not included in the calculations, such as direct breakup and transfers, are much larger for ^{6}Li than for ^{7}Li.

DOI: 10.1103/PhysRevC.87.054606 PACS number(s): 25.70.Bc, 25.70.Hi, 24.10.Eq

I. INTRODUCTION

The influence of breakup on the elastic scattering and fusion for systems involving weakly bound nuclei at energies around the Coulomb barrier has been widely studied in the last decades (see, e.g., Refs. [1–3]).

Useful information about effects of couplings to various channels on the fusion cross section may be obtained from the barrier distribution extracted from the measured fusion excitation function. The fusion barrier distribution has been defined by Rowley *et al.* [4] as

$$D_{\rm fus}(E) = \frac{d^2}{dE^2}[E\sigma_{\rm fus}(E)]. \quad (1)$$

The extraction of the barrier distribution by taking the second derivative of the quantity $E\sigma_{\rm fus}(E)$ with respect to E requires very precise measurements of the fusion cross sections.

Similar information on the role of the channel couplings in the fusion process can be obtained from the measurement of quasielastic (QEL) scattering at backward angles [5–7]. QEL scattering is defined as the sum of elastic and inelastic scattering, and all other direct processes, such as transfer and breakup. Fusion is related to the probability of transmission through the barrier for angular momentum $L = 0$, $T_0(E)$, and large-angle QEL scattering is related to the reflection probability, $R_0(E)$. Because of the conservation of the reaction flux, $T_0(E) + R_0(E) = 1$, QEL backscattering can be considered as complementary to fusion. The barrier distribution of QEL scattering ($D_{\rm qel}$) is defined as [7]

$$D_{\rm qel}(E) = -\frac{d}{dE}\left[\frac{d\sigma_{\rm qel}}{d\sigma_{\rm Ruth}}(E)\right], \quad (2)$$

where $(d\sigma_{\rm qel}/d\sigma_{\rm Ruth})$ is the ratio of the QEL scattering and Rutherford differential cross sections at a fixed backward angle. Another representation of barrier distribution was proposed in Ref. [8],

$$D_{\rm el}(E) = -\frac{d}{dE}\left[\sqrt{\frac{d\sigma_{\rm el}}{d\sigma_{\rm Ruth}}(E)}\right], \quad (3)$$

where $(d\sigma_{\rm el}/d\sigma_{\rm Ruth})$ is the ratio of the elastic scattering and Rutherford differential cross sections at a fixed backward angle. The advantage of these methods is that they require numerical evaluation of first derivatives rather than second derivatives as in the case of fusion. Furthermore, in most cases, it is easier to measure QEL/elastic scattering than fusion cross sections.

The barrier distribution method has been applied to many heavy-ion systems involving tightly bound nuclei [9] (for more recent studies see, e.g., Ref. [10] and references therein). The barrier distributions from QEL and elastic scattering for several systems have been compared with those derived from fusion (see, e.g., Refs. [11,12]). These comparisons showed that $D_{\rm el}$ and $D_{\rm qel}$ are similar to $D_{\rm fus}$ for tightly bound systems.

In reactions with weakly bound projectiles the breakup channel is expected to play an important role. The projectile breakup may be accompanied by a process called incomplete fusion (ICF) [1], where part of the broken projectile is absorbed by the target. The process where none of the breakup fragments is captured by the target is called noncapture breakup (NCBU). If the QEL cross section includes NCBU and ICF, the distribution $D_{\rm qel}$ can be associated with the complete fusion (CF) barrier distribution [13]. If only NCBU is included in the QEL cross section, the distribution $D_{\rm qel}$ is equivalent to that derived from the total fusion cross section [13]. Zagrebaev recently suggested [14] that, if the breakup processes, and possibly other important reaction channels, are not included in

*zadro@irb.hr

 ©2013 American Physical Society

the QEL cross section, the distribution $D_{\rm qel}$, extracted from the elastic + inelastic backscattering, provides information about the "total-reaction threshold distribution," and not about the fusion barriers (see also Ref. [15]).

Several studies of fusion barrier distributions for systems with weakly bound projectiles have been reported about a decade ago [16–19]. QEL and elastic-scattering barrier distributions for systems involving weakly bound nuclei have been studied only recently [12,20–26], with the exception of Ref. [17].

Signorini *et al.* [17] found that the barrier distribution for ^{9}Be + ^{209}Bi obtained from elastic-scattering data, as defined by Eq. (3), is broader than that derived from CF data. Lin *et al.* [12] measured the excitation functions of QEL and elastic scattering at backward angles for the systems ^{6,7}Li + ^{208}Pb. It was shown that the barrier distributions extracted from the excitation functions of the QEL scattering, including breakup, are almost the same as those extracted from the CF excitation functions. Jia *et al.* [26] compared the barrier distribution extracted from the sum of elastic and inelastic scattering with the CF barrier distribution for ^{9}Be + ^{208}Pb. It was found that the effects of breakup in the QEL scattering are large.

The experimental QEL-scattering excitation functions and barrier distributions for the ^{6}Li + ^{144}Sm [20] and ^{6}Li + ^{232}Th [21] systems were analyzed within the coupled-channel (CC) model. It was shown that sequential breakup of ^{6}Li through the first resonant state is an important channel to be included in the calculations, but it is not enough to reproduce the data. In Ref. [22] the large-angle QEL-scattering data for the ^{7}Li + ^{144}Sm and ^{6}Li + ^{144}Sm systems were compared with continuum discretized coupled-channel (CDCC) calculations. It was concluded that in order to explain the measured excitation functions and the extracted barrier distributions the breakup channel has to be included in calculations.

References [23–25] report on measurements of elastic backscattering excitation functions for ^{6,7}Li projectiles on ^{28}Si, ^{58}Ni, ^{116,120}Sn, and ^{208}Pb targets. The experimental barrier distributions were used to constrain the energy dependence of the optical potential at near- and sub-barrier energies. The CDCC calculations show that the effects of coupling to continuum are large for ^{6}Li and much smaller for ^{7}Li.

In summary, excitation functions for QEL and/or elastic scattering at backward angles have been measured, and corresponding barrier distributions derived, for several systems involving the weakly bound nuclei ^{6,7}Li and ^{9}Be. Usually, the experimental data have been analyzed within the CC or CDCC models. The results show that the barrier distribution method is a useful tool to study the effects of coupling among different reaction channels at near-barrier energies.

With the aim to further investigate the dynamics of reactions induced by weakly bound nuclei, we have recently started a systematic study of the ^{6,7}Li + ^{64}Zn systems at energies around the Coulomb barrier. We already measured the ^{6}Li + ^{64}Zn elastic-scattering angular distributions at $E_{\rm c.m.} \approx 11$–18 MeV [27]. The experimental data were analyzed within the optical model to study the energy dependence of the interaction potential. The results obtained suggest the presence of a breakup-threshold anomaly, usually explained as due to the strong coupling to the breakup channel. We also measured the total fusion cross sections for these systems in the energy range $E_{\rm c.m.} \approx 9$–28 MeV [28]. It has been observed that heavy residue production is dominated by CF at above-barrier energies whereas processes like ICF and/or transfer become dominant at sub-barrier energies.

In the present article we describe the measurement of the backward-angle QEL-scattering excitation functions and the corresponding barrier distributions for the ^{6,7}Li + ^{64}Zn systems at energies $8 \lesssim E_{\rm c.m.} \lesssim 18$ MeV. Furthermore, we analyze these experimental data in the framework of CC calculations.

This article is organized as follows: In Sec. II we present the experimental details and experimental results for the excitation functions and barrier distributions. In Sec. III we compare these results with CC calculations. In Sec. IV we discuss our results. Summary and conclusions are given in Sec. V.

II. EXPERIMENTAL DETAILS

A. Experimental setup

The measurements were performed at the Laboratori Nazionali del Sud, INFN, in Catania, Italy. The ^{6}Li and ^{7}Li beams were delivered by the SMP Tandem Van de Graaff accelerator.

The target was 99.4% enriched ^{64}Zn evaporated onto a $\sim$15 μg/cm^2 thick carbon backing. The target thickness was $\sim$140 μg/cm^2 in the ^{6}Li + ^{64}Zn experiment and $\sim$70 μg/cm^2 in the ^{7}Li + ^{64}Zn experiment. A thin ^{209}Bi backing layer, 2–5 μg/cm^2, was also present in the targets. Backscattering events were detected and charge identified by four silicon telescopes. The telescopes were mounted at approximately $\pm160^\circ$ and $\pm170^\circ$ relative to the beam direction. The angular opening of these telescopes with respect to the target center was 1.5° and 1.8°, respectively. Two monitor telescopes placed at $\pm25^\circ$, with an angular opening of $\sim$0.2°, were used for normalization purposes. Two additional monitor telescopes, with an angular opening of $\sim$0.6°, were set at $\pm45^\circ$. Each telescope consisted of a $\sim$10-μm-thick ΔE detector followed by an E detector with a thickness in the range 100–500 μm. The stability of the electronics was continuously controlled during the whole measurement using a precise pulse generator.

The beam was defined by a circular collimator with a diameter of 1.5 mm, placed 17 cm upstream of the target, and a rectangular aperture of 3 × 3 mm^2, located 155 cm upstream of the target. Beam currents varied from 2 to 10 pnA. The length of the measurements at low energies was such that the statistical error of the number of counts in the elastic peak at $\pm170^\circ$ was $\sim$1%. For the highest energies the cross sections at backward angles are very small and the statistical uncertainties were $\sim$7%.

Excitation functions of QEL scattering were measured in the energy range $E_{\rm lab} = 9$–20 MeV in steps of 0.5 MeV. In the ^{6}Li + ^{64}Zn experiment the point at 19.5 MeV was not measured.

B. Data analysis and results

Figure 1 shows a typical two-dimensional ΔE versus residual energy $E_{\rm res}$ spectrum for the ^{6}Li + ^{64}Zn system measured

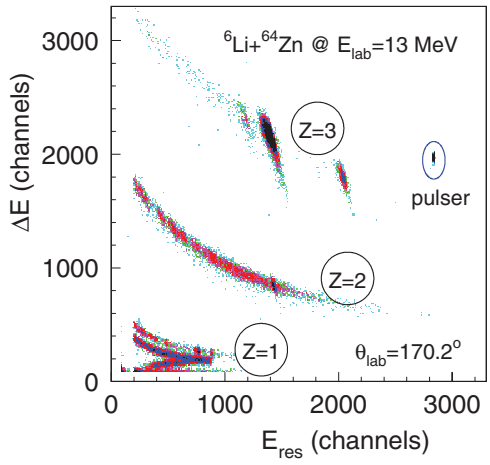

FIG. 1. (Color online) Typical ΔE-$E_{\rm res}$ spectrum for the ^{6}Li + ^{64}Zn system measured at $E_{\rm lab} = 13$ MeV, $\theta_{\rm lab} = 170.2^\circ$.

at 13 MeV with the telescope placed at $\theta_{\rm lab} = 170.2^\circ$. Events corresponding to $Z = 1$, 2, and 3 can be clearly separated. Figure 2 shows the projection on the total-energy axis for events associated with $Z = 3$. The peaks corresponding to the elastic and inelastic scattering to the 0.99 MeV 2^+ state of ^{64}Zn could be resolved and are well separated from the scattering on ^{209}Bi.

A two-dimensional spectrum ΔE-E for events corresponding to $Z = 3$ from the ^{7}Li + ^{64}Zn reaction at $E_{\rm lab} = 16$ MeV and $\theta_{\rm lab} = 170.2^\circ$ is shown in Fig. 3. The events corresponding to the elastic scattering and inelastic scattering to the 0.48 MeV $1/2^-$ state of ^{7}Li and the 0.99 MeV 2^+ state of ^{64}Zn, as well as ^{64}Zn(^{7}Li,^{6}Li)^{65}Zn one-neutron ($1n$) transfer are clearly visible.

The mass resolution of the telescopes was not good enough to separate ^{6}Li from ^{7}Li. However, the transfer to the the low-lying states of ^{65}Zn with excitations $E_{\rm x} < 0.21$ MeV is kinematically well separated from the elastic and inelastic scattering. (The Q value for the $1n$ stripping between the ground states is +0.73 MeV.)

For the events associated with $Z = 3$, the Q-value spectra for the ^{6,7}Li + ^{64}Zn scattering were calculated using two-body

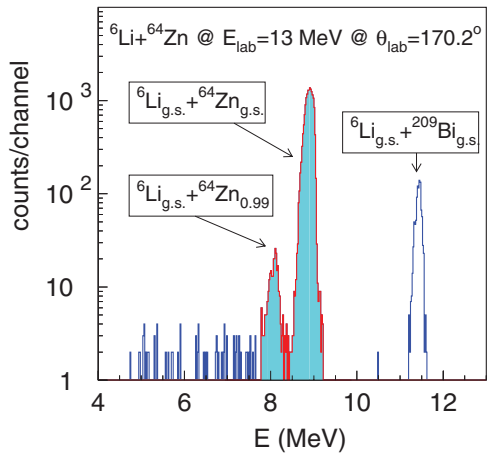

FIG. 2. (Color online) Projection of events with $Z = 3$ of Fig. 1 on the total-energy axis.

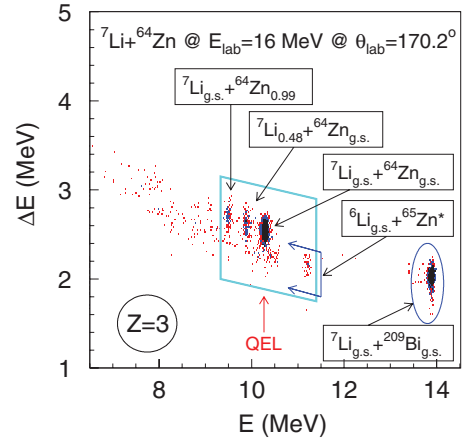

FIG. 3. (Color online) Two-dimensional ΔE-E spectrum for events with $Z = 3$ from the ^{7}Li + ^{64}Zn reaction at $E_{\rm lab} = 16$ MeV, $\theta_{\rm lab} = 170.2^\circ$.

kinematics. Then the spectra were integrated over a Q-value window that includes the events of interest. In the case of the ^{6}Li + ^{64}Zn reaction the elastic scattering and inelastic excitation of the ^{64}Zn 2^+ state were included. In the case of ^{7}Li + ^{64}Zn, the QEL scattering was defined as the sum of the elastic scattering, inelastic excitation of the ^{7}Li $1/2^-$ and ^{64}Zn 2^+ states, and $1n$ transfer to the ^{65}Zn states. The excitations of ^{65}Zn covered by the QEL Q-value window were in the range from 0 to ∼2.2–2.5 MeV, depending on the angle and beam energy. The QEL events for the case shown in Fig. 3 are indicated by the box.

The events with $Z = 1$ and $Z = 2$ may come from different reaction channels, such as noncapture breakup, incomplete fusion, transfer, and evaporation, as well as from reactions with carbon backing and target impurities. Since it was not possible to identify clearly the origins of these events, they were not considered in the analysis of QEL processes.

Absolute values of the QEL cross sections were obtained by assuming that the scattering at ±25°, where two monitor detectors were placed, is pure Rutherford. At lower energies, the elastic-scattering events corresponding to ^{64}Zn and ^{209}Bi were not separated for these forward angles. The number of counts corresponding to the ^{6,7}Li + ^{209}Bi scattering in the forward monitors was then determined from the scattering in the monitors placed at ±45°, by assuming that the ^{6,7}Li + ^{209}Bi scattering is pure Rutherford for all monitor detectors.

The ratios of the solid angles between monitors and telescopes were determined by the Rutherford scattering of ^{6}Li and ^{7}Li on a gold target at low energies. The ratio of the QEL scattering to the Rutherford cross section is obtained from the expression

$$\frac{d\sigma_{\rm qel}}{d\sigma_{\rm Ruth}}(\theta_{\rm tel}) = \left[\frac{N_{\rm tel}(\theta_{\rm tel})}{N_{\rm mon}(\theta_{\rm mon})}\right]\left[\frac{(d\sigma_{\rm Ruth}/d\Omega)(\theta_{\rm mon})}{(d\sigma_{\rm Ruth}/d\Omega)(\theta_{\rm tel})}\right]\left[\frac{\Delta\Omega_{\rm mon}}{\Delta\Omega_{\rm tel}}\right], \quad (4)$$

where

$$\left[\frac{\Delta\Omega_{\rm mon}}{\Delta\Omega_{\rm tel}}\right] = \left[\frac{N^{\rm Au}_{\rm mon}(\theta_{\rm mon})}{N^{\rm Au}_{\rm tel}(\theta_{\rm tel})}\right]\left[\frac{(d\sigma_{\rm Ruth}/d\Omega)^{\rm Au}(\theta_{\rm tel})}{(d\sigma_{\rm Ruth}/d\Omega)^{\rm Au}(\theta_{\rm mon})}\right]. \quad (5)$$

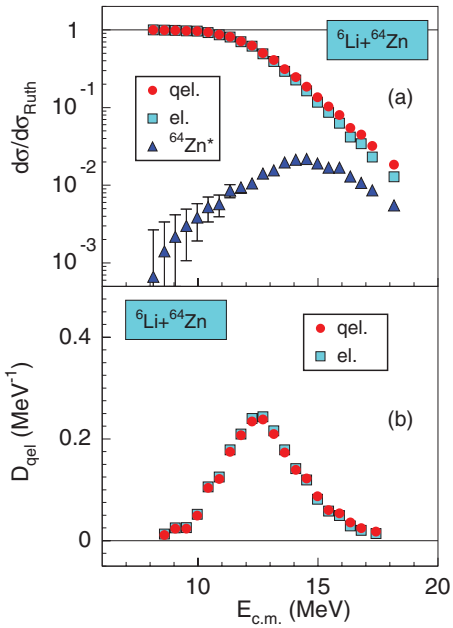

FIG. 4. (Color online) (a) Ratio of measured backward-angle cross sections to Rutherford cross sections for elastic (filled squares), inelastic ^{64}Zn(2_1^+) (filled triangles), and quasielastic (filled circles) scattering for ^{6}Li + ^{64}Zn system. (b) Barrier distributions derived from the elastic and quasielastic excitation functions.

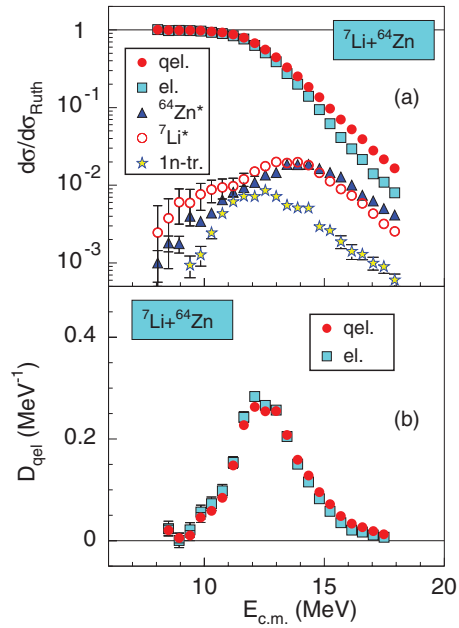

FIG. 5. (Color online) (a) Ratio of measured backward-angle cross sections to Rutherford cross sections for elastic (filled squares), inelastic ^{64}Zn(2_1^+) (filled triangles), inelastic ^{7}Li($1/2_1^-$) (empty circles), and quasielastic (filled circles) scattering and $1n$ transfer to the low-lying states of ^{65}Zn (stars) for ^{7}Li + ^{64}Zn system. (b) Barrier distributions derived from elastic and quasielastic excitation functions.

Here, $N_{\rm mon}(\theta_{\rm mon})$ and $N_{\rm tel}(\theta_{\rm tel})$ are the number of detected events in the monitor detector (at angle $\theta_{\rm mon}$) and telescope (at angle $\theta_{\rm tel}$), respectively, and $\Delta\Omega_{\rm mon}$ and $\Delta\Omega_{\rm tel}$ are the corresponding solid angles. The superscript Au refers to the ^{6,7}Li + ^{197}Au scattering.

The QEL barrier distribution can be obtained from the QEL backward scattering excitation function by using Eq. (2). The cross section appearing in Eq. (2) should be at $\theta_{\rm c.m.} \sim 180^\circ$. Therefore, the center-of-mass energies $E_{\rm c.m.}$ were corrected by the angle-dependent centrifugal potential (see, e.g., Ref. [7]). The final QEL scattering cross sections as a function of $E_{\rm c.m.}$ (the mean value of the energies corrected by the centrifugal potential at the detector angles) were obtained by averaging the cross sections for the four detectors at $\theta_{\rm tel} = \pm 160^\circ$ and $\pm 170^\circ$. The first derivative of the experimental excitation functions in Eq. (2) were obtained by using a least-squares linear fit method [29]. The straight lines are fit to three successive experimental points and the derivatives are obtained from the slopes of these lines.

As mentioned in Sec. I, since not all relevant reaction channels are included in the QEL processes, the derived barrier distribution does not correspond to the fusion barrier distribution, but reflects the reaction threshold distribution [14]. However, we will focus here on the effects of couplings between different reaction channels at near-barrier energies and not on the relations between distributions given by Eqs. (1), (2), and (3).

Figures 4 and 5 show the measured excitation functions and barrier distributions for the ^{6}Li + ^{64}Zn and ^{7}Li + ^{64}Zn systems, respectively. [It should be noted that the barrier distribution corresponding to the elastic-scattering excitation function was derived using the same relation as for the QEL scattering, Eq. (2), for the purpose of easier comparison between the elastic and QEL scattering data.] One observes that the effect of nonelastic processes on the barrier distribution is a very slight shift to higher energies and a decrease of its height.

At the lowest energies the inelastic-scattering cross section is small compared to the background originating from the tail of the elastic peak. The background under the inelastic peak(s) was estimated from the neighboring part of the spectrum, on the left side of the peak(s), and subtracted. Furthermore, the elastic and its adjacent inelastic peak were not well separated at the lowest energies. Therefore, the estimated uncertainties in the peak separation were included in the experimental errors of the cross sections for the inelastic excitation of the target in Fig. 4 and projectile in Fig. 5. The errors shown for the other excitation functions in Figs. 4 and 5 are only statistical.

As noted above, the elastic- and inelastic-scattering events for the ^{7}Li + ^{64}Zn system cannot be separated from the $1n$ transfer events. Because of that the extracted cross sections for inelastic scattering could be overestimated due to the $1n$ transfer "background" by ∼10–20%. The elastic-scattering cross sections for ^{7}Li + ^{64}Zn were extracted from the spectra measured with the telescopes at $+160^\circ$ and -170° for which the overlap of the ^{6}Li and ^{7}Li events was somewhat smaller. The uncertainty in the extracted cross sections due to the $1n$ transfer background increases with energy and could amount to 8% at the highest energies.

III. COUPLED-CHANNEL CALCULATIONS

The experimental data for QEL excitation functions and barrier distributions were analyzed within the coupled-channel (CC) method. The calculations were carried out using the code FRESCO [30].

Two low-lying collective states of the target were included in the CC calculations: the 2^+ state at 0.992 MeV and the 3^- state at 2.998 MeV. For the ^{6}Li projectile, the 3^+ (2.186 MeV) and 2^+ (4.312 MeV) unbound resonant states were taken into account. For the ^{7}Li projectile, we included the first-excited state $1/2^-$ (0.478 MeV) and the resonant state $7/2^-$ (4.652 MeV).

The diagonal potential used in the CC calculations has the following form:

$$V(r) = V_{\rm C}(r) + V_{\rm bare}(r) + i\,W_{\rm bare}(r), \tag{6}$$

where $V_{\rm C}(r)$ is the Coulomb potential, and $V_{\rm bare}(r) + i\,W_{\rm bare}(r)$ is the nuclear "bare" potential. The Coulomb potential of a uniformly charged sphere with radius $R_{\rm C} = 1.25 \times (A_P^{1/3} + A_T^{1/3})$, where A_P and A_T are the mass numbers of the projectile and target, respectively, was used as $V_{\rm C}(r)$. The real part of the bare potential was taken to be the double-folding potential, $V_{\rm bare}(r) = V_{\rm DF}(r)$,

$$V_{\rm DF}(r) = \iint d\mathbf{r}_P d\mathbf{r}_T \rho_P(r_P)\rho_T(r_T) v_{NN}(|\mathbf{r} + \mathbf{r}_T - \mathbf{r}_P|), \tag{7}$$

where $\rho_P(r_P)$ and $\rho_T(r_T)$ are the projectile and target ground-state densities, respectively, and v_{NN} is the effective nucleon-nucleon interaction.

For v_{NN} we used the M3Y-Reid interaction with the zero-range exchange term in the energy-independent form [31]. The matter densities for ^{6}Li and ^{64}Zn were derived from the charge distributions for these nuclei by assuming that the neutrons and protons are distributed similarly [31]. The charge distribution for ^{6}Li was taken from Ref. [32] and for ^{64}Zn we used a two-parameter Fermi (2pF) distribution from Refs. [33,34]. The matter density of ^{7}Li was taken from Ref. [35]. The double-folding potentials were calculated using the code DEPOT [36].

The imaginary part of the bare potential was of Woods-Saxon form with parameters [44] $W_0 = 50$ MeV, $R_W = 1.0 \times (A_P^{1/3} + A_T^{1/3})$ fm, and $a_W = 0.3$ fm. This very-short-range imaginary potential simulates the ingoing-wave boundary condition to account for the fusion process [45].

The nuclear coupling potentials for inelastic scattering were also obtained by the double-folding method, using Eq. (7) but with a transition density replacing the ground-state density of the excited nucleus and with the ground-state density of the other nucleus. A simple derivative form was used for the radial part of the transition density (see, e.g., Ref. [46]),

$$\rho_{if}^{\lambda}(r) = -\delta_{if}^{\lambda}\frac{d}{dr}\rho^0(r), \tag{8}$$

where $\rho^0(r)$ is the ground-state density, δ_{if}^{λ} is the nuclear deformation length for transition between states i and f, and λ is the multipolarity of the transition.

The Coulomb reduced matrix elements $\langle J_f \| E\lambda \| J_i \rangle$ were obtained from the experimental values of the reduced transition probability $B(E\lambda)$ (see Refs. [30,47]). The deformation lengths for nuclear transitions were derived from the Coulomb matrix elements assuming a collective model and that the neutron and proton distributions have the same shape and the same deformation lengths. The rotational model gives for a rotational band with band-head K

$$\langle J_f \| E\lambda \| J_i \rangle = \delta_{if}^{\lambda}\sqrt{2J_i + 1}\langle J_i K, \lambda 0 | J_f K\rangle \frac{(\lambda + 2)Z\langle r_p^{\lambda-1}\rangle}{4\pi}, \tag{9}$$

$$\langle r_p^{\lambda-1}\rangle = \frac{\int \rho_p^0(r) r^{\lambda+1} dr}{\int \rho_p^0(r) r^2 dr}, \tag{10}$$

where $\rho_p^0(r)$ is the proton part of the ground state density (see also Refs. [46,47]). Reorientation couplings were also taken into account. The diagonal matrix elements $\langle J \| E2 \| J \rangle$ were obtained from the spectroscopic electric quadrupole moments Q_s, when available, or from the nondiagonal matrix elements assuming a rotational model. The parameters relevant for the present CC calculations are summarized in Table I.

The QEL excitation functions were calculated at the same energies and angles for which the experimental cross sections were measured and the theoretical barrier distributions were derived using the same procedure that was applied to the experimental data.

Results of the CC calculations are compared with experimental data in Figs. 6 and 7. The dotted lines in these figures represent the results of the calculations without any coupling. The thin solid lines are the results of the CC calculations taking into account the inelastic channels included in the experimental QEL cross sections: the excitation of the ^{64}Zn 2_1^+ state in the case of the ^{6}Li + ^{64}Zn system and the ^{64}Zn 2_1^+ and ^{7}Li $1/2_1^-$ states in the case of the ^{7}Li + ^{64}Zn system. The reorientation of the target 2_1^+ excited state and projectile $3/2_1^-$ ground state were also taken into account. The thick solid lines represent the results when the couplings to the projectile resonant state(s) and the target 3_1^- state are also included in the calculations.

The no-coupling calculations are far from the experimental data for both the excitation functions and the barrier distributions. When the target 2_1^+ excited state is included in calculations the agreement with the experimental data is not much better, as can be seen in Fig. 6 for the ^{6}Li + ^{64}Zn system. By including the couplings to the ^{6}Li resonant states and the ^{64}Zn 3_1^- state the results for the QEL excitation function change significantly. However, the agreement with the experimental excitation function is still poor and the influence of these channels on the barrier distribution is small. Note that for the ^{7}Li + ^{64}Zn system the cross sections for the inelastic excitation of the ^{7}Li first-excited state are also included in the QEL cross sections. The inclusion of this channel and the reorientation of the ^{7}Li ground state in the CC calculations moves the predictions in the correct direction. In particular, the agreement with the experimental barrier distribution improves significantly. The influence of the included channels is to reduce the height and broaden the barrier distribution. However, the height is still overestimated. The thick solid curves in Fig. 7 show the results when the couplings to the ^{64}Zn 3_1^- excited state and the ^{7}Li $7/2_1^-$ resonant state are also considered. The inclusion of these

TABLE I. Experimental values of quadrupole moments Q_s and reduced transition probabilities $B(E\lambda)$ used in the present CC analysis for the calculations of the Coulomb matrix elements and nuclear deformation lengths δ_{ij}^{λ} for inelastic transitions in ^{6}Li, ^{7}Li, and ^{64}Zn. $(\delta_{ij}^{\lambda})_{\rm expt}$ are "experimental" deformation lengths for ^{6}Li [37].

Nucleus	Transition $(J_i \to J_f)$	λ	Q_s (e fm^2)	$B(E\lambda, J_i \to J_f)$ (e^2 fm$^{2\lambda}$)	Ref.	δ_{if}^{λ} (fm)	$(\delta_{if}^{\lambda})_{\rm expt}$ (fm)
^{6}Li	$(1^+ \to 1^+)$	2	−0.0806		[38]	−0.122	−0.76
	$(1^+ \to 3^+)$	2		25.6	[39]	−3.854	−2.04
	$(3^+ \to 3^+)$[a]	2				−3.854	−1.53
	$(1^+ \to 2^+)$	2		7.9	[39]	−1.915	−1.95
	$(2^+ \to 2^+)$[a]	2				−1.915	−0.98
^{7}Li	$(3/2^- \to 3/2^-)$	2	−4.00		[38,40]	2.961	
	$(3/2^- \to 1/2^-)$	2		7.27	[40]	2.830	
	$(3/2^- \to 7/2^-)$	2		17.5	[41]	2.738	
	$(7/2^- \to 7/2^-)$[a]	2				2.738	
^{64}Zn	$(0^+ \to 2^+)$	2		1680	[42]	1.163	
	$(2^+ \to 2^+)$	2	−32		[42]	1.002	
	$(0^+ \to 3^-)$	3		34000	[43]	1.023	

[a]Coulomb matrix elements for these reorientation terms are determined from $B(E2)$ assuming the rotational model.

couplings improves the prediction for the QEL excitation function and has a small effect on the barrier distribution.

It should be noted that the contribution of the $1n$ transfer channel (^{7}Li, ^{6}Li) was included in the experimental QEL excitation function, but was not included in our calculations. It can be seen from Fig. 5 that the contribution of the transfer to the low-lying states of ^{65}Zn, $E_x < 0.21$ MeV, to the QEL excitation function is small. However, as can be seen from Fig. 3, the contribution of the transfer to the ^{65}Zn states with higher excitations, $E_x \gtrsim 0.8$ MeV, might be appreciable. In any case, the effects of the transfer channel couplings on the elastic and inelastic scattering cannot be excluded.

As noted in several papers, e.g., Refs. [37,48,49], the deformation length for the transition $1_1^+ \to 3_1^+$ in ^{6}Li derived from the reduced transition probability $B(E2)$ is much larger than the values obtained in different CC analyses of ^{6}Li scattering. Figure 8 shows the results of calculations for the ^{6}Li + ^{64}Zn system obtained by using the nuclear deformation lengths taken from Ref. [37], where they were adjusted to fit the ^{6}Li scattering data. By comparing with results of Fig. 6, one can observe that the agreement between the calculations and the data worsened. This suggests that disagreement between CC calculations and data for ^{6}Li is presumably caused by other effects; not by the uncertainties in the deformation lengths.

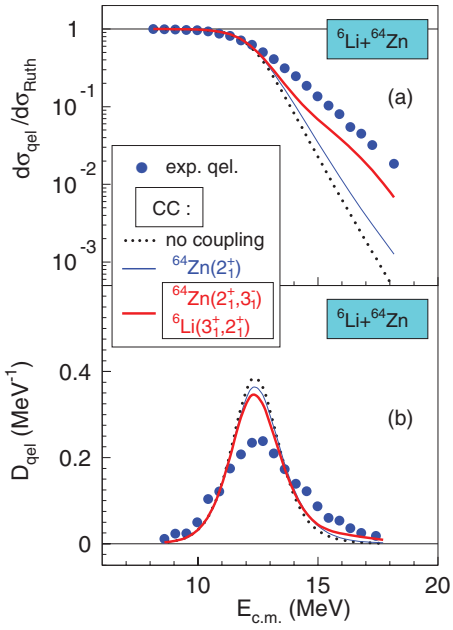

FIG. 6. (Color online) (a) Quasielastic backscattering excitation function and (b) quasielastic barrier distribution for ^{6}Li + ^{64}Zn system. The lines are results of CC calculations (see text for details).

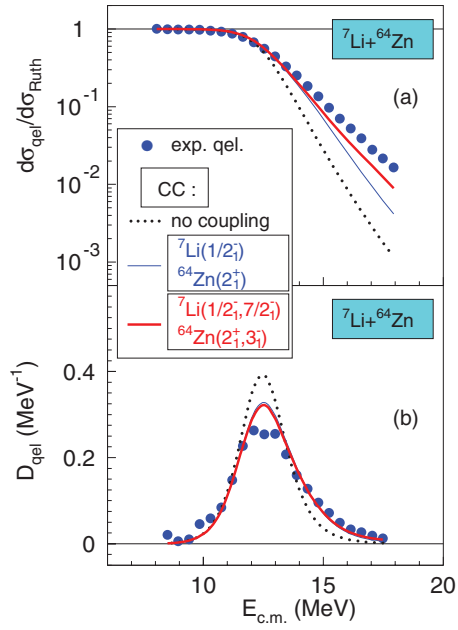

FIG. 7. (Color online) (a) Quasielastic backscattering excitation function and (b) quasielastic barrier distribution for ^{7}Li + ^{64}Zn system. The lines are results of CC calculations (see text for details).

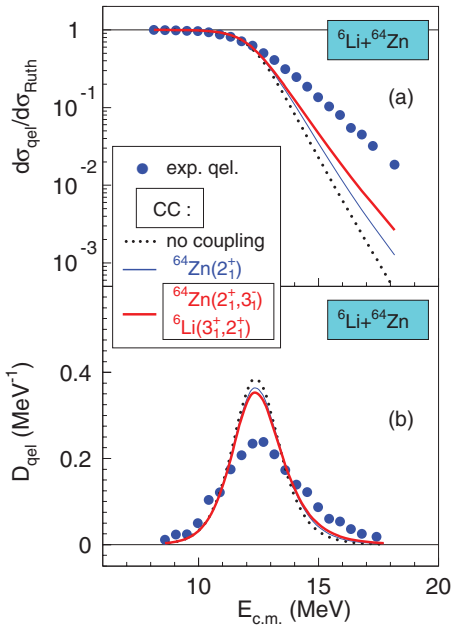

FIG. 8. (Color online) (a) Quasielastic backscattering excitation function and (b) quasielastic barrier distribution for ^{6}Li + ^{64}Zn system. The lines represent the CC calculations using "experimental" deformation lengths for transitions in ^{6}Li (see text for details).

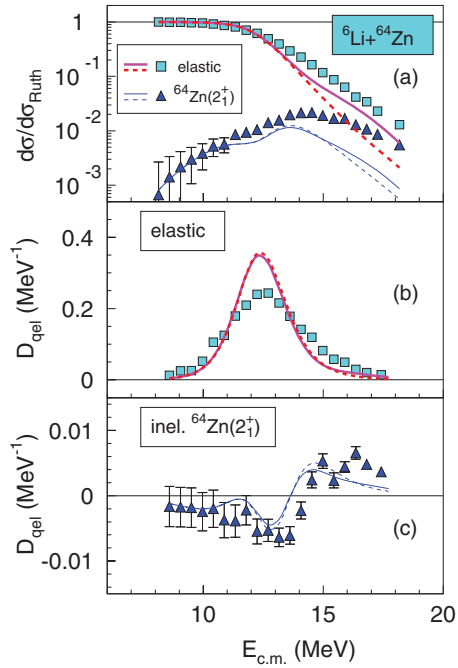

FIG. 9. (Color online) (a) Excitation functions of elastic (filled squares) and inelastic ^{64}Zn(2^+_1) (filled triangles) backscattering and corresponding contributions to the QEL barrier distribution in panels (b) and (c), respectively, for ^{6}Li + ^{64}Zn system. The lines represent the CC calculations using deformation lengths obtained from the Coulomb matrix elements (solid lines) and "experimental" deformation lengths (dashed lines) for transitions in ^{6}Li (see text for details).

We have also derived the components of the QEL barrier distributions from the excitation functions for inelastic channels. The elastic- and inelastic-scattering excitation functions obtained from the CC calculations and the corresponding "partial" barrier distributions are compared with the experimental data in Figs. 9 and 10.

For the ^{6}Li + ^{64}Zn system, the CC calculations obtained by using two different sets of deformation lengths for transitions in ^{6}Li are shown in Fig. 9. As in the QEL case, the calculations do not reproduce the experimental data, neither for the elastic nor for the inelastic scattering.

For the ^{7}Li + ^{64}Zn system the agreement of the CC calculations with the experimental excitation function for elastic scattering is better than for QEL scattering. The agreement with the experimental barrier distributions for the elastic scattering is similar to that for the QEL scattering, and it is much better than for the the case of the ^{6}Li projectile. The agreement for the target ^{64}Zn(2^+_1) inelastic scattering seems reasonable, for both the excitation function and barrier distribution, as the experimental cross sections are probably overestimated. On the other hand, the calculations do not reproduce well the experimental data for the ^{7}Li($1/2^-_1$) inelastic scattering. Better agreement for the elastic-scattering excitation function compared with the QEL case is due to the very small cross sections predicted for this inelastic channel and partially to the contribution of the $1n$ transfer channel to the experimental QEL cross sections.

IV. DISCUSSION

It is important to mention that we used a bare nuclear potential, consisting of a double-folding real and a short-range imaginary part. We did not use any surface imaginary potential. Therefore, all nonelastic processes which occur at the nuclear surface should be taken into account explicitly. We considered the relevant inelastic excitations of the projectile and target with coupling strengths taken from the literature. Discrepancies between our CC calculations and experimental results for excitation functions and corresponding barrier distributions could then be attributed to the effects of the channels not taken into account in the CC calculations, such as transfers and direct breakup reactions. The ^{6}Li and ^{7}Li nuclei have the pronounced cluster structure $\alpha + d$ and $\alpha + t$, respectively, with low cluster separation energy: $S_\alpha = 1.47$ MeV for ^{6}Li and 2.47 MeV for ^{7}Li. Therefore, the breakup and/or cluster transfer channels are expected to be important.

Comparison of Fig. 7 with Figs. 6 or 8, and of Fig. 10 with Fig. 9, shows that the CC calculations for the ^{7}Li + ^{64}Zn system agree better with the data than for ^{6}Li + ^{64}Zn. One also observes that the barrier distribution for the ^{6}Li + ^{64}Zn system is broader than that for ^{7}Li + ^{64}Zn. The observed differences could be ascribed to different effects of the couplings to breakup and/or transfer channels, smaller for ^{7}Li than for ^{6}Li.

The above conclusions are consistent with recent theoretical calculations for elastic scattering [50] and (quasi)elastic scattering and barrier distributions [22–25]. Theoretical CDCC calculations for the ^{6,7}Li + ^{59}Co reactions at near-barrier energies indicate that the breakup cross sections are a small fraction of the total reaction cross sections but the coupling

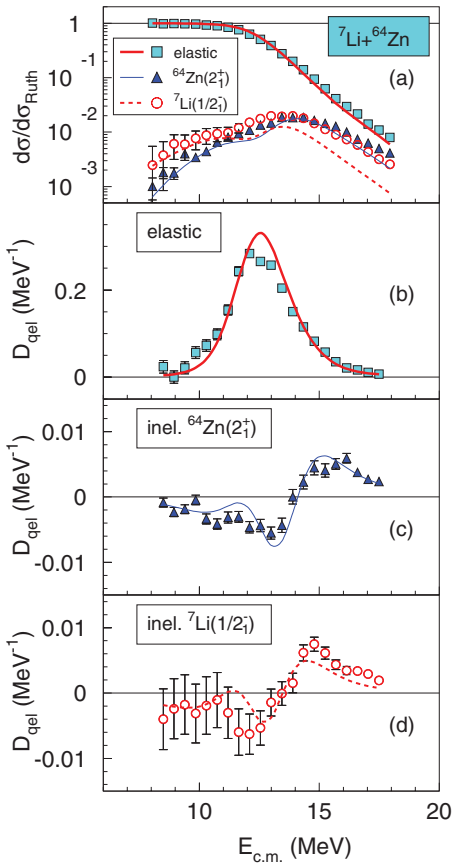

FIG. 10. (Color online) (a) Excitation functions of elastic (filled squares), inelastic ^{64}Zn(2^+_1) (filled triangles), and inelastic ^{7}Li($1/2^-_1$) (empty circles) backscattering and the corresponding contributions to the QEL barrier distribution in panels (b), (c), and (d), respectively, for ^{7}Li + ^{64}Zn system. The lines are results of CC calculations.

to the breakup channel has an important effect on the elastic scattering [50]. The influence of breakup on the elastic channel is stronger for ^{6}Li than ^{7}Li. In Refs. [22–25] the effects of breakup on (quasi)elastic scattering and the corresponding barrier distributions have been studied for different targets within the CDCC method. It was found that these effects are large for ^{6}Li and small for ^{7}Li.

Results of recent investigations of the breakup processes in the ^{6,7}Li + ^{65}Cu [51], ^{6,7}Li + ^{208}Pb [52], and ^{7}Li + ^{209}Bi [53] reactions show that the breakup following nucleon transfer is the dominant breakup mechanism at sub-barrier energies (see also Ref [54]). The channels that could be important for our systems are, for example, the (^{6}Li, ^{5}Li) one-neutron stripping ($Q = 2.32$ MeV), the (^{6}Li,^{5}He) one-proton stripping ($Q = -0.49$ MeV), and the (^{7}Li, ^{8}Be) one-proton pickup ($Q = 9.54$ MeV) followed by the breakup of the unbound nuclei ^{5}Li, ^{5}He, and ^{8}Be, respectively.

Hence, our CC calculations should be extended by including direct breakup (by using CDCC), transfer channels, and transfers followed by breakup, within coupled reaction channels (CRCs). Furthermore, the simultaneous analysis of experimental angular distributions, excitation functions, and corresponding barrier distributions for different reaction channels could help to better understand the reaction mechanisms of the weakly bound ^{6}Li and ^{7}Li nuclei at near-barrier energies.

V. SUMMARY AND CONCLUSIONS

The QEL excitation functions at backward angles have been measured for the ^{6,7}Li + ^{64}Zn systems and the corresponding barrier distributions were derived. The experimental cross sections and barrier distributions have been compared with the results of coupled-channel calculations using a double-folding bare potential. The nuclear transition potentials were also double-folding potentials calculated with a transition density of the corresponding nucleus. Inelastic excitations of the target, excitation of the ^{7}Li first-excited state, and sequential breakup through the ^{6,7}Li resonant state(s) were considered in the calculations. The discrepancies between the experimental data and the CC calculations which include two main collective states of the target, 2^+ and 3^-, are large. In the case of the ^{7}Li + ^{64}Zn system the inclusion of the reorientation of the ^{7}Li ground state and excitation of its first-excited state improve the agreement with the data, particularly for the barrier distribution. In the case of the ^{6}Li + ^{64}Zn system, the coupling to the ^{6}Li resonant states improves the predictions but the agreement with the experimental data is still very poor for both the excitation function and the corresponding barrier distribution.

The discrepancies between CC calculations and experimental data suggest that some important reaction channels were not taken into account. Couplings to the direct breakup, transfer channels, as well as breakup triggered by transfer might be responsible for the observed disagreements.

ACKNOWLEDGMENTS

We acknowledge L. Prepolec for his help in the data analysis. M.M., V.O., and M.Z. would like to thank the LNS for the hospitality and financial support.

[1] L. F. Canto, P. R. S. Gomes, R. Donangelo, and M. S. Hussein, Phys. Rep. **424**, 1 (2006).

[2] V. Scuderi, A. Di Pietro, P. Figuera, M. Fisichella, F. Amorini, C. Angulo, G. Cardella, E. Casarejos, M. Lattuada, M. Milin, A. Musumarra, M. Papa, M. G. Pellegriti, R. Raabe, F. Rizzo, N. Skukan, D. Torresi, and M. Zadro, Phys. Rev. C **84**, 064604 (2011).

[3] A. Di Pietro, V. Scuderi, A. M. Moro, L. Acosta, F. Amorini, M. J. G. Borge, P. Figuera, M. Fisichella, L. M. Fraile, J. Gomez-Camacho, H. Jeppesen, M. Lattuada, I. Martel, M. Milin, A. Musumarra, M. Papa, M. G. Pellegriti, F. Perez-Bernal, R. Raabe, G. Randisi, F. Rizzo, G. Scalia, O. Tengblad, D. Torresi, A. M. Vidal, D. Voulot, F. Wenander, and M. Zadro, Phys. Rev. C **85**, 054607 (2012).

[4] N. Rowley, G. R. Satchler, and P. H. Stelson, Phys. Lett. B **254**, 25 (1991).

[5] M. V. Andres, N. Rowley, and M. A. Nagarajan, Phys. Lett. B **202**, 292 (1988).

[6] A. T. Kruppa, P. Romain, M. A. Nagarajan, and N. Rowley, Nucl. Phys. A **560**, 845 (1993).

[7] H. Timmers, J. R. Leigh, M. Dasgupta, D. J. Hinde, R. C. Lemmon, J. C. Mein, C. R. Morton, J. O. Newton, and N. Rowley, Nucl. Phys. A **584**, 190 (1995).

[8] N. Rowley, H. Timmers, J. R. Leigh, M. Dasgupta, D. J. Hinde, J. C. Mein, C. R. Morton, and J. O. Newton, Phys. Lett. B **373**, 23 (1996).

[9] M. Dasgupta, D. J. Hinde, N. Rowley, and A. M. Stefanini, Annu. Rev. Nucl. Sci. **48**, 401 (1998).

[10] E. Piasecki, Ł. Świderski, N. Keeley, M. Kisieliński, M. Kowalczyk, S. Khlebnikov, T. Krogulski, K. Piasecki, G. Tiourin, M. Sillanpää, W. H. Trzaska, and A. Trzcińska, Phys. Rev. C **85**, 054608 (2012).

[11] H. Timmers, J. R. Leigh, N. Rowley, A. M. Stefanini, D. Ackermann, S. Beghini, L. Corradi, M. Dasgupta, J. H. He, D. J. Hinde, J. C. Mein, G. Montagnoli, C. R. Morton, J. O. Newton, F. Scarlassara, and G. F. Segato, J. Phys. G **23**, 1175 (1997).

[12] C. J. Lin, H. Q. Zhang, F. Yang, M. Ruan, Z. H. Liu, Y. W. Wu, X. K. Wu, P. Zhou, C. L. Zhang, G. L. Zhang, G. P. An, H. M. Jia, and X. X. Xu, Nucl. Phys. A **787**, 281 (2007).

[13] J. Lubian, T. Correa, P. R. S. Gomes, and L. F. Canto, Phys. Rev. C **78**, 064615 (2008).

[14] V. I. Zagrebaev, Phys. Rev. C **78**, 047602 (2008).

[15] D. S. Monteiro, P. R. S. Gomes, and J. Lubian, Phys. Rev. C **80**, 047602 (2009).

[16] M. Dasgupta, D. J. Hinde, R. D. Butt, R. M. Anjos, A. C. Berriman, N. Carlin, P. R. S. Gomes, C. R. Morton, J. O. Newton, A. Szanto de Toledo, and K. Hagino, Phys. Rev. Lett. **82**, 1395 (1999).

[17] C. Signorini, Z. H. Liu, Z. C. Li, K. E. G. Löbner, L. Müller, M. Ruan, K. Rudolph, F. Soramel, C. Zotti, A. Andrighetto, L. Stroe, A. Vitturi, and H. Q. Zhang, Eur. Phys. J. A **5**, 7 (1999).

[18] M. Dasgupta, D. J. Hinde, K. Hagino, S. B. Moraes, P. R. S. Gomes, R. M. Anjos, R. D. Butt, A. C. Berriman, N. Carlin, C. R. Morton, J. O. Newton, and A. Szanto de Toledo, Phys. Rev. C **66**, 041602(R) (2002).

[19] M. Dasgupta, P. R. S. Gomes, D. J. Hinde, S. B. Moraes, R. M. Anjos, A. C. Berriman, R. D. Butt, N. Carlin, J. Lubian, C. R. Morton, J. O. Newton, and A. Szanto de Toledo, Phys. Rev. C **70**, 024606 (2004).

[20] D. S. Monteiro, O. A. Capurro, A. Arazi, J. O. Fernández Niello, J. M. Figueira, G. V. Martí, D. Martínez Heimann, A. E. Negri, A. J. Pacheco, V. Guimarães, D. R. Otomar, J. Lubian, and P. R. S. Gomes, Phys. Rev. C **79**, 014601 (2009).

[21] S. Mukherjee, B. K. Nayak, D. S. Monteiro, J. Lubian, P. R. S. Gomes, S. Appannababu, and R. K. Choudhury, Phys. Rev. C **80**, 014607 (2009).

[22] D. R. Otomar, J. Lubian, P. R. S. Gomes, D. S. Monteiro, O. A. Capurro, A. Arazi, J. O. Fernández Niello, J. M. Figueira, G. V. Martí, D. Martinez Heimann, A. E. Negri, A. J. Pacheco, V. Guimarães, and L. C. Chamon, Phys. Rev. C **80**, 034614 (2009).

[23] K. Zerva, N. Patronis, A. Pakou, N. Alamanos, X. Aslanoglou, D. Filipescu, T. Glodariu, M. Kokkoris, M. La Commara, A. Lagoyannis, M. Mazzocco, N. G. Nicolis, D. Pierroutsakou, M. Romoli, and K. Rusek, Phys. Rev. C **80**, 017601 (2009).

[24] K. Zerva, A. Pakou, K. Rusek, N. Patronis, N. Alamanos, X. Aslanoglou, D. Filipescu, T. Glodariu, N. Keeley, M. Kokkoris, M. La Commara, A. Lagoyannis, M. Mazzocco, N. G. Nicolis, D. Pierroutsakou, and M. Romoli, Phys. Rev. C **82**, 044607 (2010).

[25] K. Zerva, A. Pakou, N. Patronis, P. Figuera, A. Musumarra, A. Di Pietro, M. Fisichella, T. Glodariu, M. La Commara, M. Lattuada, M. Mazzocco, M. G. Pellegriti, D. Pierroutsakou, A. M. Sanchez-Benitez, V. Scuderi, E. Strano, and K. Rusek, Eur. Phys. J. A **48**, 102 (2012).

[26] H. M. Jia, C. J. Lin, H. Q. Zhang, Z. H. Liu, N. Yu, F. Yang, F. Jia, X. X. Xu, Z. D. Wu, S. T. Zhang, and C. L. Bai, Phys. Rev. C **82**, 027602 (2010).

[27] M. Zadro, P. Figuera, A. Di Pietro, F. Amorini, M. Fisichella, O. Goryunov, M. Lattuada, C. Maiolino, A. Musumarra, V. Ostashko, M. Papa, M. G. Pellegriti, F. Rizzo, D. Santonocito, V. Scuderi, and D. Torresi, Phys. Rev. C **80**, 064610 (2009).

[28] A. Di Pietro, P. Figuera, E. Strano, M. Fisichella, O. Goryunov, M. Lattuada, C. Maiolino, C. Marchetta, M. Milin, A. Musumarra, V. Ostashko, M. G. Pellegriti, V. Privitera, G. Randisi, L. Romano, D. Santonocito, V. Scuderi, D. Torresi, and M. Zadro (unpublished).

[29] O. A. Capurro, J. E. Testoni, D. Abriola, D. E. DiGregorio, G. V. Martí, A. J. Pacheco, M. R. Spinella, and E. Achterberg, Phys. Rev. C **62**, 014613 (2000).

[30] I. J. Thompson, Comput. Phys. Rep. **7**, 167 (1988).

[31] G. R. Satchler and W. G. Love, Phys. Rep. **55**, 183 (1979).

[32] G. C. Li, I. Sick, R. R. Witney, and M. R. Yearian, Nucl. Phys. A **162**, 583 (1971).

[33] R. Neuhausen, J. W. Lightbody, Jr., S. P. Fivozinsky, and S. Penner, Phys. Rev. C **5**, 124 (1972).

[34] C. W. De Jager, H. De Vries, and C. De Vries, At. Data Nucl. Data Tables **14**, 479 (1974).

[35] J. Cook, M. F. Vineyard, K. W. Kemper, and V. Hnizdo, Phys. Rev. C **27**, 1536 (1983).

[36] J. Cook, Comput. Phys. Commun. **25**, 125 (1982).

[37] P. L. Kerr, K. W. Kemper, P. V. Green, K. Mohajeri, E. G. Myers, B. G. Schmidt, and V. Hnizdo, Phys. Rev. C **54**, 1267 (1996).

[38] D. Borremans, D. L. Balabanski, K. Blaum, W. Geithner, S. Gheysen, P. Himpe, M. Kowalska, J. Lassen, P. Lievens, S. Mallion, R. Neugart, G. Neyens, N. Vermeulen, and D. Yordanov, Phys. Rev. C **72**, 044309 (2005).

[39] F. Eigenbrod, Z. Phys. **228**, 1969 (1969).

[40] H.-G. Voelk and D. Fick, Nucl. Phys A **530**, 475 (1991).

[41] R. M. Hutcheon and H. S. Caplan, Nucl. Phys A **127**, 417 (1969).

[42] S. Salém-Vasconcelos, M. J. Bechara, J. H. Hirata, and O. Dietzsch, Phys. Rev. C **38**, 2439 (1988).

[43] T. Kibédi and R. H. Spear, At. Data Nucl. Data Tables **80**, 35 (2002).

[44] N. Keeley, R. Raabe, N. Alamanos, and J. L. Sida, Prog. Part. Nucl. Phys. **59**, 579 (2007).

[45] M. J. Rhoades-Brown and P. Braun-Munzinger, Phys. Lett. B **136**, 19 (1984).

[46] Dao T. Khoa and G. R. Satchler, Nucl. Phys A **668**, 3 (2000).

[47] I. J. Thompson and F. M. Nunes, *Nuclear Reactions for Astrophysics* (Cambridge University Press, Cambridge, 2009).

[48] S. P. Van Verst, D. P. Sanderson, D. E. Trcka, K. W. Kemper, V. Hnizdo, B. G. Schmidt, and K. R. Chapman, Phys. Rev. C **39**, 853 (1989).

[49] E. L. Reber, K. W. Kemper, P. V. Green, P. L. Kerr, A. J. Mendez, E. G. Myers, B. G. Schmidt, and V. Hnizdo, Phys. Rev. C **50**, 2917 (1994).

[50] C. Beck, N. Keeley, and A. Diaz-Torres, Phys. Rev. C **75**, 054605 (2007).

[51] A. Shrivastava, A. Navin, N. Keeley, K. Mahata, K. Ramachandran, V. Nanal, V. V. Parkar, A. Chatterjee, and S. Kailas, Phys. Lett. B **633**, 463 (2006).

[52] D. H. Luong, M. Dasgupta, D. J. Hinde, R. du Rietz, R. Rafiei, C. J. Lin, M. Evers, and A. Diaz-Torres, Phys. Lett. B **695**, 105 (2011); D. H. Luong, D. J. Hinde, M. Dasgupta, M. Evers, R. Rafiei, and R. du Rietz, EPJ Web Conf. **17**, 03002 (2011).

[53] M. Dasgupta, L. R. Gasques, D. H. Luong, R. du Rietz, R. Rafiei, D. J. Hinde, C. J. Lin, M. Evers, and A. Diaz-Torres, Nucl. Phys. A **834**, 147c (2010).

[54] P. R. S. Gomes, D. R. Otomar, T. Correa, L. F. Canto, J. Lubian, R. Linares, D. H. Luong, M. Dasgupta, D. J. Hinde, and M. S. Hussein, J. Phys. G **39**, 115103 (2012).